

Introducing Open Boundary Conditions in Modeling Nonperiodic Materials and Interfaces: The Impact of the Periodicity Assumption

James Charles,* Sabre Kais, and Tillmann Kubis



Cite This: *ACS Materials Lett.* 2020, 2, 247–253



Read Online

ACCESS |



Metrics & More

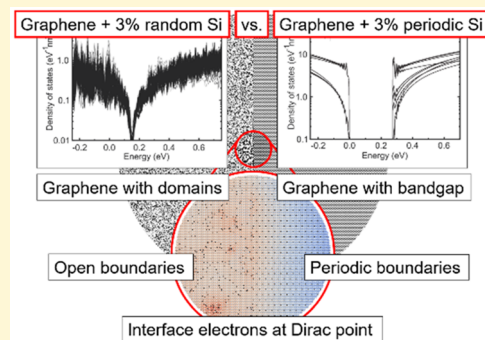


Article Recommendations



Supporting Information

ABSTRACT: Simulations are essential to accelerate the discovery of new materials and to gain full understanding of known ones. Although hard to realize experimentally, periodic boundary conditions are omnipresent in material simulations. In this work, we introduce ROBIN (recursive open boundary and interfaces), the first method allowing open boundary conditions in material and interface modeling. The computational costs are limited to solving quantum properties in a focus area that allows explicitly discretizing millions of atoms in real space and to consider virtually any type of environment (be it periodic, regular, or random). The impact of the periodicity assumption is assessed in detail with silicon dopants in graphene. Graphene was confirmed to produce a band gap with periodic substitution of 3% carbon with silicon in agreement with published periodic boundary condition calculations. Instead, 3% randomly distributed silicon in graphene only shifts the energy spectrum. The predicted shift agrees quantitatively with published experimental data. Key insight of this assessment is, assuming periodicity elevates a small perturbation of a periodic cell into a strong impact on the material property prediction. Periodic boundary conditions can be applied on truly periodic systems only. More general systems should apply an open boundary method for reliable predictions.



Computer-aided material predictions represent the first-step of many new material discoveries.^{1–3} Material simulations can power machine learning searches for new materials with specific properties.^{4–6} However, modeling experimental reality with wide-spread idealized, periodic boundary conditions^{7,8} is prone to artifacts: Irregular interfaces, impurities, cracks and dislocations are not compatible with idealized conditions. A common approach to limit artificial periodicity effects is to make the repeating unit cell as large as numerically feasible and apply various correction algorithms.^{9–12}

Instead, we introduce the recursive open boundary and interfaces (ROBIN) method, which can handle arbitrary geometries and atom distributions and does not need any periodicity assumption. It is based on the nonequilibrium Green's function method (NEGF). The NEGF method had been applied on charge,^{13,14} spin,^{15,16} and heat^{17,18} transport in open nanodevices. The ROBIN extension of NEGF models materials in infinitely extended real space and supports regular and irregular systems. We verify the ROBIN method in 2D and 3D crystalline systems. To assess the impact of periodic

boundary conditions on material property predictions, an as-simple-as-possible but experimentally realized system was chosen: Calculations of graphene confirm recent work¹⁹ that periodically distributed silicon impurities can open bandgaps. In stark contrast and presumably closer to any experiment, random distributions of the same amount of silicon are shown to give no band gaps but to form domains and to linearly shift the band structure. The predicted shift quantitatively agrees with experimental data of ref 19. The findings of ROBIN are analyzed in detail and show that periodic boundary conditions can elevate otherwise small perturbations to systematic changes of material properties.

So far, all models for quantum electronic material properties are based on Hermitian Hamiltonian operators (H) that represent either periodic or finite-sized systems.²⁰ The

Received: December 9, 2019

Accepted: February 10, 2020

Published: February 10, 2020

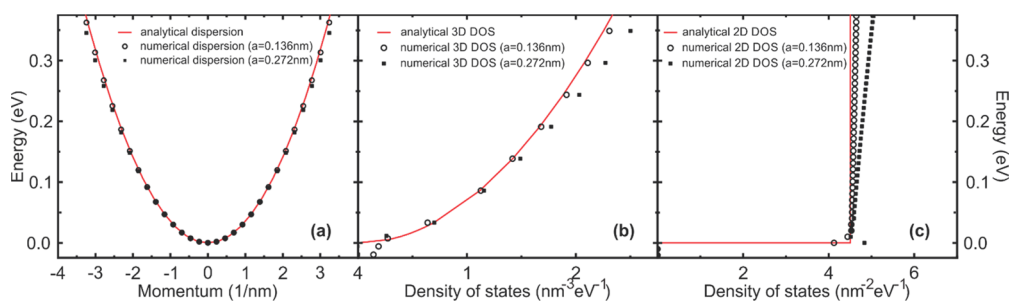


Figure 1. Verification of the ROBIN method against analytical results: (a) The analytical dispersion of effective mass electrons (line) and the numerical dispersion of periodic Hamiltonian operators discretized in a real space mesh of 0.136 (circles) and 0.272 nm (dots) mesh point distance are known to deviate more with higher kinetic energies. Similarly, the numerical density of states of open system simulations with ROBIN (symbols) deviates from the analytical one (lines) with higher energies and larger mesh constants, both in 3D (b) and 2D (c). Otherwise, all results of the ROBIN method resemble the expected analytical data very well.

boundaries of closed systems yield confinement effects and system size dependent resonances that can interfere with the actual material properties. Models with periodic boundary conditions require numerically hard to achieve unit cell sizes to avoid artificial long-distance coupling between repeating simulation domain features.²¹ To lift some of the numerical limitations of periodic simulations, various correction methods have been introduced.^{11,22,23} The k -space sampling required for periodic boundary simulations represents additional numerical challenges.²⁰ Modeling systems with long distance effects, such as Moiré lattices, systems with irregularities, such as alloys, and systems with inhomogeneous fields or strain are notoriously difficult to handle with Hermitian Hamiltonian operators.

In the NEGF method, the electronic density of states (DOS) equals the imaginary part of the retarded Green's function's (G^R) diagonal. G^R is solved in the Dyson equation, which reads in operator form $G^R = (E - H_C - \Sigma^R)^{-1}$, with the electronic energy E , and the retarded self-energy Σ^R .²⁴ The Hermitian Hamiltonian H_C represents the electrons in the finite, central area C . We set C to be a sphere for three-dimensional and a circle for two-dimensional systems. However, any other space-appropriate shapes are possible, too. Electrons are modeled in the effective mass approximation²⁵ when the ROBIN method is verified against analytical DOS of parabolic dispersions in 2D and 3D. In case of graphene, electrons are given in single-orbital atomistic tight binding ($E_{p_z,C} = 0$, $V_{pp\sigma,C} = 0$, $V_{pp\pi} = -3$ eV), following the nomenclature of ref 26 on the native graphene lattice. Silicon atoms in graphene are modeled with graphene parameters and an on-site energy of $E_{p_z,Si} = 4.75$ eV to reproduce the band gap of 3% periodically distributed Si in graphene predicted with DFT in ref 19. Note that many other electronic representations, such as plane waves,²⁷ maximally localized Wannier functions,^{28,29} or localized atomic orbitals,^{30,31} have been applied in NEGF before. Devices modeled in NEGF covered 1D, 2D, and 3D symmetries, ranging from molecular junctions³² up to micrometer long resistors.³³

The retarded self-energy Σ^R is the key element that distinguishes NEGF from closed-system models: It is the non-Hermitian operator in the inverse G^R that represents the interaction of electrons in C with the surrounding of C at the contact interface between the two regions.³⁴ Σ^R allows electrons to enter and leave C at the contact and then to propagate to infinite distance to C . The imaginary part of Σ^R is inverse proportional to the electronic lifetime in C (i.e., the "dwelling-in- C -time").³⁵

Most NEGF applications require the surrounding "behind" the contact to form a homogeneous lead and in particular to have a well-defined 1D transport direction. A few exceptions to this limitation can be found for quantum cascade systems^{13,36} and recent transistor predictions.³⁷ Ref 37, in particular, allowed for the lead cross section size to grow infinitely with increasing distance to the contact and to host random atom distributions.

The ROBIN method expands the contact self-energy method of ref 37 by considering the total interface between C and the surrounding as the contact area. The conceptual difference to ref 37 is the fact that only one contact self-energy describes the complete environment. Following ref 37, the non-Hermitian Σ^R is solved as a product of the non-Hermitian surface retarded Green's function of the 2D or 3D surrounding of C with the Hermitian Hamiltonian operators of atoms in C coupling with atoms in the surrounding. Thereby, the environment atoms are discretized explicitly. A complex absorbing potential (CAP) is added to the environmental atoms' on-site energies.³⁸ Similar to that in ref 37, the CAP vanishes at the edges of C and grows smoothly with increasing distance to C .³⁹ The CAP is critical to ensure efficient convergence of the results in C with the range of explicitly discretized surrounding atoms.

The numerical costs solving for the retarded Green's functions is the largest challenge of the ROBIN method. Therefore, all retarded Green's functions are solved recursively^{40,41} to limit the required peak memory and to allow for explicit consideration of up to 3 million atoms in this work. Many publications^{42–46} and online lectures^{47,48} on recursive Green's functions describe the method in high detail. Details of the CAP method are discussed in refs 37 and 49. All ROBIN calculations have been performed on 10 nodes of the Brown cluster of the Rosen Center for Advanced Computing at Purdue University.

Since all density of states results of open system calculations come with a continuous DOS, smoothing spectral results as needed in Hermitian models is obsolete here.^{50–52} Although this work covers only electronic examples, the presented method applies to any system with discretizable equations of motion, including, for example, lattice vibrations in dynamic matrix descriptions.

Figure 1 verifies the ROBIN method for electronic material property predictions. Figure 1a is a reminder of the electronic dispersion resulting of electronic Hamiltonian operators of silicon conduction band electrons ($m^* = 1.08m_0$) discretized in real space and solved with periodic boundary conditions. Note

this is the only periodic-boundary system result, while all remaining results apply the ROBIN method of open boundaries. Deviations from the analytical parabolic dispersion become smaller with decreasing kinetic energies and finer mesh spacing.⁵³ Accordingly, with finer real space meshes and smaller kinetic energies the DOS of the ROBIN method in 3D (Figure 1b) and 2D (Figure 1c) agree better with the respective analytical DOS, that is, the square root function in 3D and the constant DOS in 2D.

Similar to the Si nanowire calculations in ref 19, the convergence of Σ^R close to band edges is more demanding and small deviations from the analytical DOS can be observed there. Better convergence further reduces the DOS deviation at the band edge.

This convergence also determines the quality of the predicted DOS at the Dirac point of graphene. Figure 2 shows the average DOS of graphene electrons solved in graphene discs of varying diameters. The center region C is chosen to be a disc of 1 nm diameter for all results in Figure 2.

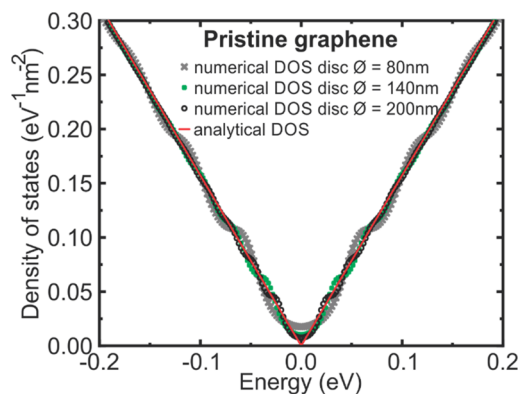


Figure 2. Verification of the ROBIN method against analytical results: The numerical density of states resulting of the ROBIN method (symbols) of graphene discs agree better with the analytical density of states (line) with larger discretized disc diameter.

All remaining carbon atoms are included as part of the environment of C within the ROBIN method. In this way, the largest disc size considered in Figure 2 is 200 nm diameter, which includes more than 1 million discretized carbon atoms in total. The average DOS in Figure 2 converges well to the linear dispersion of graphene with increasing lead size. Simultaneously, the standard deviation of the DOS of each considered atom in C versus the depicted average value reduces, too. The maximum of this standard deviation for all considered energies in Figure 2 is 1.2×10^{-4} (80 nm), 1.5×10^{-5} (140 nm), and $6.3 \times 10^{-7} \text{ eV}^{-1} \text{ nm}^{-2}$ (200 nm), respectively.

In ref 19, a 3% concentration of periodically distributed silicon atoms in graphene was analyzed with density functional theory calculations and periodic boundary conditions. It was predicted that the addition of the silicon atoms opens a bandgap of 0.28 eV in graphene. This finding can be reproduced with the ROBIN method in empirical tight binding: All Si atoms are considered periodically distributed in the graphene disc. Silicon parameters are approximated with graphene parameters and an additional on-site energy of 4.75 eV. Given the unit cell is larger with the periodic Si than in the case of pristine graphene (see Figure 3), the convergence of

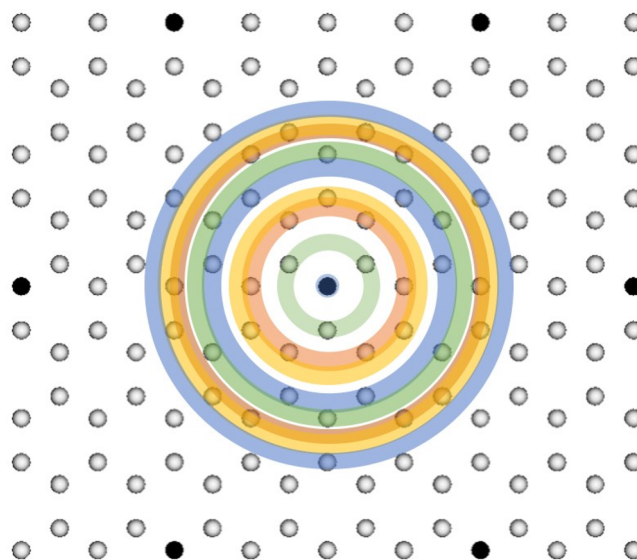


Figure 3. Schematic of carbon (white) and silicon (black) atoms in graphene with 3% periodically distributed silicon. Nine different atom types are in each unit cell: one silicon atom and carbon atoms in 8 different distances to the central silicon, highlighted by 8 semi-transparent rings around the center Si circle.

the DOS w.r.t the disc diameter is numerically more challenging. This can be seen in the slowly decaying beating pattern in Figure 4a. Even a disc diameter of 320 nm with more than 3 million discretized atoms still shows a small beating in the resulting DOS around the band gap. Figure 4a shows the electronic DOS of each of 282 atoms of a 3 nm center area of two different graphene discs (200 and 320 nm diameter) solved with the ROBIN method.

The periodic distribution of carbon (white) and 3% silicon (black) atoms is shown in Figure 3. The addition of silicon atoms increases the graphene unit cell to 32 atoms that fall into 9 different chemical categories: 1 silicon atom and 8 graphene atoms in 8 different distances to the silicon one (see Figure 3). Accordingly, a ROBIN prediction of the atom resolved DOS of graphene with 3% periodically distributed Si yields 9 different DOS lines—as shown in Figure 4a. Note that Figure 4a actually shows 282 individual DOS lines for each of the 282 atoms in the 3 nm center region. Good convergence of the contact self-energy makes them virtually identical to DOS lines of atoms with the same chemical environment (see Figure 4b for a zoom-in).

The DOS changes significantly when the 3% silicon atoms are randomly distributed (see Figure 4c). The 282 local DOS lines of each atom in the center region C differ depending on their respective local atomic environment. The ensemble of atomic DOS lines maintains a Dirac point at about $\Delta E = 0.147 \text{ eV}$ above the Dirac point of pristine graphene. Note that ΔE scales approximately linearly with the % fraction of randomly distributed Si atoms in graphene as can be seen in Figure 4c for the 1% and 2% Si cases. For comparison, Figure 4c also shows the analytical DOS of pristine graphene.

Adding only 1%, 2%, or 3% silicon should only perturb graphene within the linear response regime. Indeed, the ROBIN results in Figure 4c for this amount of randomly distributed Si show only a linear shift of the Dirac cone. Periodic boundary conditions of the same small amount of Si atoms give a dramatic change to the graphene band structure,

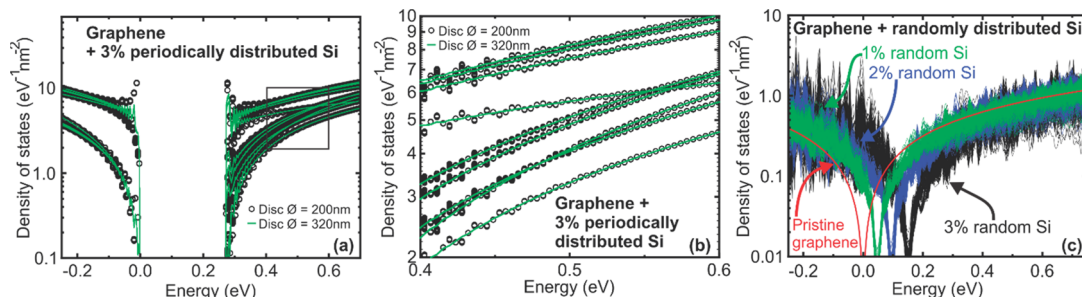


Figure 4. (a) Density of states of graphene with 3% periodically distributed silicon solved with the ROBIN method reproduces the 0.28 eV band gap of ref 19 when the on-site energy of Si is chosen as 4.75 eV. The large unit cell of 3% Si in graphene burdens the numerical convergence w.r.t the disc diameter. 200 nm (symbols) and, to lesser extent, the 320 nm (lines) disc diameter show incomplete convergence near the band gap. (b) Zoom-in into the boxed region in panel a. The 282 individual atoms of the calculation in panel a fall into 9 distinct groups of DOS lines, corresponding to the 9 different atom types shown in Figure 3. (c) The DOS solved in the ROBIN method of randomly distributed Si atoms in graphene does not show a bandgap. Instead, increasing Si content shifts the DOS to higher energies by about 47 meV per Si-percentage (i.e., about 1% of the assumed on-site energy difference of carbon and silicon atoms). The red line shows the analytical DOS of pristine graphene for comparison.

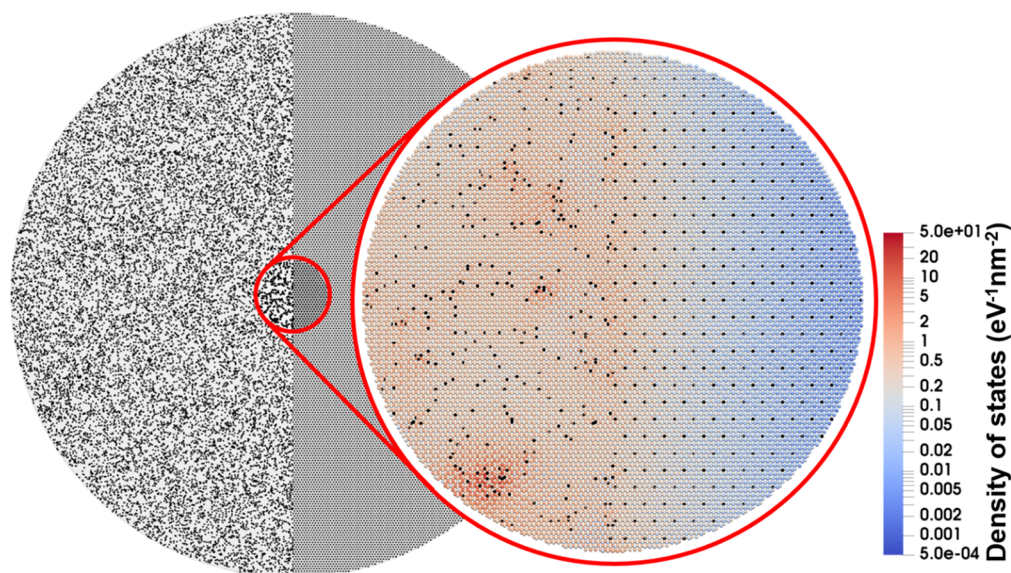


Figure 5. (left) 200 nm disc of graphene (carbon atoms are white) with 3% Si atoms (black) distributed randomly on the left and periodically on the right half of the disc. (right) Electronic density of states of the center 25 nm of the 200 nm graphene disc solved with open boundary conditions at 10 meV above the Dirac point of pristine graphene. Carbon atoms are colored according to the electronic DOS, and the silicon atoms are black. The electronic DOS shows domain formation in the left half and electronic tunneling into the right half of the disc.

resembling effectively a new material. In other words, applying periodic boundary conditions elevates otherwise small perturbations to systematic material property changes. Therefore, periodic boundary conditions should only be applied to truly periodic systems. In the experiments of ref 19, 3% randomly distributed Si in graphene yielded a shift of the electronic work function by 0.13 eV. The predicted shift of 147 meV in Figure 4c agrees quantitatively with that observation given the experimental Si concentration uncertainty of ref 19 (2.7–4.5%).

To illustrate the DOS difference of periodically and randomly distributed silicon atoms in graphene, Figure 5 shows open system results of the center 25 nm of a 200 nm diameter graphene disc with 3% silicon atoms distributed randomly on the left half and periodically on the right half of the disc. The contour shows the position resolved DOS at the energy of 10 meV above the Dirac point of pristine graphene. The black spheres indicate the position of Si atoms. Depending on local Si atom distributions, electrons on the left face pockets

of high DOS; whereas, all the DOS decays in the right are due to the bandgap opened by the periodically distributed Si.

Substituting atoms periodically is a remarkably difficult experimental task especially if single substitutions are considered. We expect random distributions to resemble the experimental reality much more closely. Given the stark contrast in electronic properties of periodic versus random distributions, materials with periodic substitutions should be considered fully distinct from the original pristine host material. This applies to substituting with other than Si atom kinds,^{54,55} as well as other host materials than graphene.

In conclusion, this work introduces the ROBIN method to predict 2D and 3D materials in arbitrary, regular, and irregular atomic compositions. Green's functions are solved recursively to explicitly discretize millions of atoms within the memory limitations of typical state of the art hardware. When applied on silicon atoms distributed in graphene, the method reveals a significant difference in the electronic properties of periodic versus randomly distributed Si atoms in graphene. The

calculations confirm periodically distributed Si atoms form bandgaps in graphene, but the same amount of randomly distributed Si atoms forms domains in the electronic DOS and shifts the graphene DOS in energy. The results show that applying periodic boundary conditions can elevate small perturbations to massively influence material property predictions.

It is worth mentioning that the ROBIN method can be applied on systems with random alloys, single defects, and interfaces. Systems involving different physical phases (e.g. heterogeneous catalysis,⁵⁶ emulsions,⁵⁷ melting solids, microdroplet chemistry,⁵⁸ etc.) are conceptually equivalent to the situation in Figure 5. To illustrate the generality of the ROBIN method, Figure S1 shows the electronic DOS at the energy of the graphene Dirac point in twisted bilayer graphene with a twist angle of 5° (a) and 30° (b), respectively. The ROBIN method is independent of whether the system is irregular, periodic, or quasi-crystalline. The data in the Figure S1 were solved with the same numerical effort and the same simulation settings. The expected periodicity and quasi-crystalline behavior is reproduced in both cases.^{59–61}

The applicability of ROBIN on 3D materials is further exemplified in Figure S2 because it shows the electronic DOS of a spherical Ge cluster embedded in Si and solved with ROBIN in sp3d5s* atomistic tight binding representation.⁶² The cluster size is chosen to be 2 nm in diameter, which is common in SiGe alloys.⁶³ The electronic DOS at 50 meV above the Si valence band edge has two maxima in the Ge cluster but leaks significantly into Si.

■ ASSOCIATED CONTENT

SI Supporting Information

The Supporting Information is available free of charge at <https://pubs.acs.org/doi/10.1021/acsmaterialslett.9b00523>.

DOS figures, S1 and S2, including the DOS of bilayer graphene and a Ge cluster embedded in Si, respectively (PDF)

■ AUTHOR INFORMATION

Corresponding Author

James Charles – School of Electrical and Computer Engineering, Purdue University, West Lafayette, Indiana 47907, United States; orcid.org/0000-0002-4212-7435; Email: charlesj@purdue.edu

Authors

Sabre Kais – Department of Physics and Astronomy and Department of Chemistry, Purdue University, West Lafayette, Indiana, United States; orcid.org/0000-0003-0574-5346

Tillmann Kubis – School of Electrical and Computer Engineering, Network for Computational Nanotechnology, and Center for Predictive Materials and Devices, Purdue University, West Lafayette, Indiana 47907, United States; Purdue Institute of Inflammation, Immunology, and Infectious Disease, West Lafayette, Indiana 47907, United States

Complete contact information is available at:

<https://pubs.acs.org/doi/10.1021/acsmaterialslett.9b00523>

Author Contributions

J.C. performed the method development and implementation, the numerical calculations, and the manuscript writing. S.K. contributed to the manuscript writing and by consultation and discussions. T.K. contributed to the method development and

implementation, the data analysis, and the manuscript writing. He supervised the project.

Funding

This research was supported by the NSF EFRI 2DARE 1433510 and through computational resources provided by Rosen Center for Advanced Computing at Purdue University, West Lafayette, Indiana.

Notes

The authors declare no competing financial interest.

The structure files with the position of C and Si atoms of Figures 4c and 5 can be freely downloaded from www.nanohub.org/resources/30959.

■ ACKNOWLEDGMENTS

During the preparation of this manuscript, we became aware of ref 64, which introduces an open system self-energy treatment for regular, pristine environments. Irregular environments, such as those that form the subject in this work are beyond ref 64, however. We acknowledge long and fruitful discussions with Prof. R. Graham Cooks of the Purdue Chemistry department.

■ ABBREVIATIONS

NEGF, nonequilibrium Green's function method; ROBIN, recursive open boundary and interfaces method; DOS, density of states

■ REFERENCES

- (1) Oganov, A. R.; Pickard, C. J.; Zhu, Q.; Needs, R. J. Structure Prediction Drives Materials Discovery. *Nat. Rev. Mater.* **2019**, *4*, 331–348.
- (2) Hafner, J.; Wolverton, C.; Ceder, G. Toward Computational Materials Design: The Impact of Density Functional Theory on Materials Research. *MRS Bull.* **2006**, *31*, 659–668.
- (3) Schleder, G. R.; Padilha, A. C. M.; Acosta, C. M.; Costa, M.; Fazzio, A. From DFT to Machine Learning: Recent Approaches to Materials Science—a Review. *J. Phys. Mater.* **2019**, *2*, No. 032001.
- (4) Iwasaki, Y.; Takeuchi, I.; Stanev, V.; Kusne, A. G.; Ishida, M.; Kirihara, A.; Ihara, K.; Sawada, R.; Terashima, K.; Someya, H.; et al. Machine-Learning Guided Discovery of a New Thermoelectric Material. *Sci. Rep.* **2019**, *9*, 2751.
- (5) Paliana, G.; Mannodi-Kanakkithodi, A.; Uberuaga, B. P.; Ramprasad, R.; Gubernatis, J. E.; Lookman, T. Machine Learning Bandgaps of Double Perovskites. *Sci. Rep.* **2016**, *6*, 19375.
- (6) Butler, K. T.; Davies, D. W.; Cartwright, H.; Isayev, O.; Walsh, A. Machine Learning for Molecular and Materials Science. *Nature* **2018**, *559*, 547–555.
- (7) Han, J.; Thomas, S. L.; Srolovitz, D. J. Grain-Boundary Kinetics: A Unified Approach. *Prog. Mater. Sci.* **2018**, *98*, 386–476.
- (8) Medasani, B.; Gamst, A.; Ding, H.; Chen, W.; Persson, K. A.; Asta, M.; Canning, A.; Haranczyk, M. Predicting Defect Behavior in B2 Intermetallics by Merging Ab Initio Modeling and Machine Learning. *Npj Comput. Mater.* **2016**, *2*, 2.
- (9) Ganduglia-Pirovano, M. V.; Da Silva, J. L. F.; Sauer, J. Density-Functional Calculations of the Structure of Near-Surface Oxygen Vacancies and Electron Localization on CeO₂(111). *Phys. Rev. Lett.* **2009**, *102*, No. 026101.
- (10) Yadav, V. K.; Chakraborty, H.; Klein, M. L.; Waghmare, U. V.; Rao, C. N. R. Defect-Enriched Tunability of Electronic and Charge-Carrier Transport Characteristics of 2D Borocarbonitride (BCN) Monolayers from Ab Initio Calculations. *Nanoscale* **2019**, *11*, 19398.
- (11) Freysoldt, C.; Neugebauer, J.; Van de Walle, C. G. Fully Ab Initio Finite-Size Corrections for Charged-Defect Supercell Calculations. *Phys. Rev. Lett.* **2009**, *102*, No. 016402.
- (12) Neugebauer, J.; Hickel, T. Density Functional Theory in Materials Science. *Wiley Interdiscip. Rev. Comput. Mol. Sci.* **2013**, *3*, 438–448.

- (13) Jirauschek, C.; Kubis, T. Modeling Techniques for Quantum Cascade Lasers. *Appl. Phys. Rev.* **2014**, *1*, No. 011307.
- (14) Steiger, S.; Povolotskiy, M.; Park, H.-H.; Kubis, T.; Klimeck, G. NEMOS: A Parallel Multiscale Nanoelectronics Modeling Tool. *IEEE Trans. Nanotechnol.* **2011**, *10*, 1464.
- (15) Zanolli, Z.; Onida, G.; Charlier, J.-C. Quantum Spin Transport in Carbon Chains. *ACS Nano* **2010**, *4*, 5174–5180.
- (16) Kim, W. Y.; Choi, Y. C.; Min, S. K.; Cho, Y.; Kim, K. S. Application of Quantum Chemistry to Nanotechnology: Electron and Spin Transport in Molecular Devices. *Chem. Soc. Rev.* **2009**, *38*, 2319–2333.
- (17) Sadasivam, S.; Ye, N.; Feser, J. P.; Charles, J.; Miao, K.; Kubis, T.; Fisher, T. S. Thermal Transport across Metal Silicide-Silicon Interfaces: First-Principles Calculations and Green's Function Transport Simulations. *Phys. Rev. B: Condens. Matter Mater. Phys.* **2017**, *95*, No. 085310.
- (18) Wang, J.-S.; Agarwalla, B. K.; Li, H.; Thingna, J. Non-equilibrium Green's Function Method for Quantum Thermal Transport. *Front. Phys.* **2014**, *9*, 673–697.
- (19) Zhang, S. J.; Lin, S. S.; Li, X. Q.; Liu, X. Y.; Wu, H. A.; Xu, W. L.; Wang, P.; Wu, Z. Q.; Zhong, H. K.; Xu, Z. J. Opening the Band Gap of Graphene through Silicon Doping for the Improved Performance of Graphene/GaAs Heterojunction Solar Cells. *Nanoscale* **2016**, *8*, 226–232.
- (20) Giannozzi, P.; Baroni, S.; Bonini, N.; Calandra, M.; Car, R.; Cavazzoni, C.; Ceresoli, D.; Chiarotti, G. L.; Cococcioni, M.; Dabo, I.; et al. QUANTUM ESPRESSO: A Modular and Open-Source Software Project for Quantum Simulations of Materials. *J. Phys.: Condens. Matter* **2009**, *21*, 395502.
- (21) Castleton, C. W. M.; Höglund, A.; Mirbt, S. Density Functional Theory Calculations of Defect Energies Using Supercells. *Modell. Simul. Mater. Sci. Eng.* **2009**, *17*, No. 084003.
- (22) Gerstmann, U.; Deák, P.; Rurai, R.; Aradi, B.; Frauenheim, Th.; Overhof, H. Charge Corrections for Supercell Calculations of Defects in Semiconductors. *Phys. B* **2003**, *340–342*, 190–194.
- (23) Lewis, D. K.; Matsubara, M.; Bellotti, E.; Sharifzadeh, S. Quasiparticle and Hybrid Density Functional Methods in Defect Studies: An Application to the Nitrogen Vacancy in GaN. *Phys. Rev. B: Condens. Matter Mater. Phys.* **2017**, *96*, 235203.
- (24) Kadanoff, L. P.; Baym, G. *Quantum Statistical Mechanics*; Pines, D., Ed.; Westview Press, 1994.
- (25) Wacker, A. Gain in Quantum Cascade Lasers and Superlattices: A Quantum Transport Theory. *Phys. Rev. B: Condens. Matter Mater. Phys.* **2002**, *66*, No. 085326.
- (26) Podolskiy, A. V.; Vogl, P. Compact Expression for the Angular Dependence of Tight-Binding Hamiltonian Matrix Elements. *Phys. Rev. B: Condens. Matter Mater. Phys.* **2004**, *69*, 233101.
- (27) Pala, M. G.; Esseni, D. Full-Band Quantum Simulation of Electron Devices with the Pseudopotential Method: Theory, Implementation, and Applications. *Phys. Rev. B: Condens. Matter Mater. Phys.* **2018**, *97*, 125310.
- (28) Kim, S.; Marzari, N. First-Principles Quantum Transport with Electron-Vibration Interactions: A Maximally Localized Wannier Functions Approach. *Phys. Rev. B: Condens. Matter Mater. Phys.* **2013**, *87*, 245407.
- (29) Szabó, Á.; Rhyner, R.; Luisier, M. Ab Initio Simulation of Single- and Few-Layer MoS_2 Transistors: Effect of Electron-Phonon Scattering. *Phys. Rev. B: Condens. Matter Mater. Phys.* **2015**, *92*, No. 035435.
- (30) Stokbro, K.; Smidstrup, S. Electron Transport across a Metal-Organic Interface: Simulations Using Nonequilibrium Green's Function and Density Functional Theory. *Phys. Rev. B: Condens. Matter Mater. Phys.* **2013**, *88*, No. 075317.
- (31) Sharma, U. S.; Shah, R.; Mishra, P. K. Electronic Structure and Transport Properties of Zigzag MoS_2 Nanoribbons. *AIP Conf. Proc.* **2017**, 140041.
- (32) Nitzan, A.; Ratner, M. A. Electron Transport in Molecular Wire Junctions. *Science* **2003**, *300*, 1384–1389.
- (33) Zeng, L.; He, Y.; Povolotskiy, M.; Liu, X.; Klimeck, G.; Kubis, T. Low Rank Approximation Method for Efficient Green's Function Calculation of Dissipative Quantum Transport. *J. Appl. Phys.* **2013**, *113*, 213707.
- (34) Datta, S. Nanoscale Device Modeling: The Green's Function Method. *Superlattices Microstruct.* **2000**, *28*, 253–278.
- (35) Wacker, A. Semiconductor Superlattices: A Model System for Nonlinear Transport. *Phys. Rep.* **2002**, *357*, 1–111.
- (36) Haldas, G.; Kolek, A.; Tralle, I. Modeling of Mid-Infrared Quantum Cascade Laser by Means of Nonequilibrium Green's Functions. *IEEE J. Quantum Electron.* **2011**, *47*, 878–885.
- (37) He, Y.; Wang, Y.; Klimeck, G.; Kubis, T. Non-Equilibrium Green's Functions Method: Non-Trivial and Disordered Leads. *Appl. Phys. Lett.* **2014**, *105*, 213502.
- (38) Muga, J. G.; Palao, J. P.; Navarro, B.; Egusquiza, I. L. Complex Absorbing Potentials. *Phys. Rep.* **2004**, *395*, 357–426.
- (39) Wang, Y.; He, Y.; Klimeck, G.; Kubis, T. Nonequilibrium Green's Function Method: Algorithm for Regular and Irregular Leads. *16th International Workshop on Computational Electronics* **2013**, 42–43.
- (40) Anantram, M.; Lundstrom, M. S.; Nikonov, D. E. Modeling of Nanoscale Devices. *Proc. IEEE* **2008**, *96*, 1511–1550.
- (41) Kazymyrenko, K.; Waintal, X. Knitting Algorithm for Calculating Green Functions in Quantum Systems. *Phys. Rev. B: Condens. Matter Mater. Phys.* **2008**, *77*, 115119.
- (42) Lake, R.; Klimeck, G.; Bowen, R. C.; Jovanovic, D. Single and Multiband Modeling of Quantum Electron Transport through Layered Semiconductor Devices. *J. Appl. Phys.* **1997**, *81*, 7845–7869.
- (43) Cauley, S.; Luisier, M.; Balakrishnan, V.; Klimeck, G.; Koh, C.-K. Distributed NEGF Algorithms for the Simulation of Nanoelectronic Devices with Scattering. *J. Appl. Phys.* **2011**, *110*, 043713.
- (44) Teichert, F.; Zienert, A.; Schuster, J.; Schreiber, M. Improved Recursive Green's Function Formalism for Quasi One-Dimensional Systems with Realistic Defects. *J. Comput. Phys.* **2017**, *334*, 607–619.
- (45) Lewenkopf, C. H.; Mucciolo, E. R. The Recursive Green's Function Method for Graphene. *J. Comput. Electron.* **2013**, *12*, 203–231.
- (46) Drouvelis, P. S.; Schmelcher, P.; Bastian, P. Parallel Implementation of the Recursive Green's Function Method. *J. Comput. Phys.* **2006**, *215*, 741–756.
- (47) Klimeck, G. *Nanoelectronic Modeling Lecture 21: Recursive Green Function Algorithm*, 2010. <https://nanohub.org/resources/8388>.
- (48) Klimeck, G. *Numerical Aspects of NEGF: The Recursive Green Function Algorithm*, 2004. <https://nanohub.org/resources/165>.
- (49) Kubis, T.; He, Y.; Andrawis, R.; Klimeck, G. General Retarded Contact Self-Energies in and beyond the Non-Equilibrium Green's Functions Method. *J. Phys.: Conf. Ser.* **2016**, *696*, No. 012019.
- (50) Brázdová, V.; Bowler, D. R. *Atomistic Computer Simulations: A Practical Guide*; John Wiley & Sons, 2013.
- (51) 7.33 ISMEAR, SIGMA tag. <https://cms.mpi.univie.ac.at/vasp/guide/node124.html> (accessed 2019-09-05).
- (52) Basiuk, V. A. Electron Smearing in DFT Calculations: A Case Study of Doxorubicin Interaction with Single-Walled Carbon Nanotubes. *Int. J. Quantum Chem.* **2011**, *111*, 4197–4205.
- (53) Supriyo, D. *Electronic Transport in Mesoscopic Systems*, Cambridge Studies in Semiconductor Physics and Microelectronic Engineering Book 3; Cambridge University Press, 1997.
- (54) Fan, X.; Shen, Z.; Liu, A. Q.; Kuo, J.-L. Band Gap Opening of Graphene by Doping Small Boron Nitride Domains. *Nanoscale* **2012**, *4*, 2157–2165.
- (55) Rani, P.; Jindal, V. K. Designing Band Gap of Graphene by B and N Dopant Atoms. *RSC Adv.* **2013**, *3*, 802–812.
- (56) Greeley, J.; Mavrikakis, M. Alloy Catalysts Designed from First Principles. *Nat. Mater.* **2004**, *3*, 810–815.
- (57) Anton, N.; Benoit, J.-P.; Saulnier, P. Design and Production of Nanoparticles Formulated from Nano-Emulsion Templates—A Review. *J. Controlled Release* **2008**, *128*, 185–199.
- (58) Girod, M.; Moyano, E.; Campbell, D. I.; Cooks, R. G. Accelerated Bimolecular Reactions in Microdroplets Studied by

Desorption Electrospray Ionization Mass Spectrometry. *Chem. Sci.* **2011**, *2*, 501–510.

(59) Moon, P.; Koshino, M.; Son, Y.-W. Quasicrystalline electronic states in 30° rotated twisted bilayer graphene. *Phys. Rev. B: Condens. Matter Mater. Phys.* **2019**, *99*, 165430.

(60) Carr, S.; Massatt, D.; Fang, S.; Cazeaux, P.; Luskin, M.; Kaxiras, E. Twistronics: Manipulating the Electronic Properties of Two-Dimensional Layered Structures through Their Twist Angle. *Phys. Rev. B: Condens. Matter Mater. Phys.* **2017**, *95*, No. 075420.

(61) Gibney, E. How ‘Magic Angle’ Graphene Is Stirring up Physics. *Nature* **2019**, *565*, 15–18.

(62) Boykin, T.; Klimeck, G.; Oyafuso, F. Valence Band Effective Mass Expressions in the Sp³d⁵s* Empirical Tight-Binding Model Applied to a New Si and Ge Parameterization. *Phys. Rev. B: Condens. Matter Mater. Phys.* **2004**, *69*, 115201.

(63) Pinto, N.; Murri, R.; Rinaldi, R. Cluster-Size Distribution of SiGe Alloys Grown by MBE. *Thin Solid Films* **1998**, *336*, 53–57.

(64) Papior, N.; Calogero, G.; Leitherer, S.; Brandbyge, M. Removing All Periodic Boundary Conditions: Efficient Non-Equilibrium Green Function Calculations. *arXiv (Cond-Mat Physics)*, 2019, 190511113. <https://arxiv.org/abs/1905.11113>.